FACTA UNIVERSITATIS
Series: **Mechanical Engineering**
https://doi.org/10.22190/FUME250304024H

Original scientific paper

PRESSURE OPTIMIZATION IN DEC SPRAY CHAMBERS: A COMPREHENSIVE STUDY ON HEAT AND MASS TRANSFER DYNAMICS

Xiaoqing Huang, Shunyao Lu, Ning Cai, Xiantai Wen

College of Energy and Power Engineering, Nanjing Institute of Technology, Nanjing, China

Abstract. *Achieving optimal contact between air and droplets is pivotal in direct evaporative cooling systems. This study presents an experimental analysis of spray cooling effectiveness in spray chambers utilizing pressure-swirl nozzles and impingement atomizing nozzle. Through the analysis of experimental data related to heat and mass transfer, the study reveals that if an optimal water supply pressure is identified, increasing the water flow rate does not necessarily enhance cooling performance. Furthermore, the study explores the impact of dry-bulb and wet-bulb temperatures of the air, as well as nozzle arrangement, on the determination of the optimal water supply pressure.*

Key words: *Direct evaporative cooling (DEC), Spray cooling efficiency, Heat and mass transfer, Optimal water supply pressure, Nozzle configuration optimization*

1. INTRODUCTION

Direct evaporative cooling (DEC) systems, which utilize the latent heat of water evaporation to lower air temperature, have emerged as energy-efficient alternatives to conventional vapor-compression air conditioning [1-3]. These systems are particularly advantageous in arid and semi-arid climates, where the wet-bulb depression is sufficient to achieve significant cooling effects [4-6]. However, the core challenge lies in optimizing air-water contact efficiency to maximize thermal performance while minimizing energy and water consumption [7-9]. This requires a nuanced understanding of spray dynamics, nozzle geometry, and environmental variables, which collectively govern heat and mass transfer mechanisms in DEC spray chambers [10, 11].

Received: March 04, 2025 / Accepted July 11, 2025
Corresponding author: Xiaoqing Huang
College of Energy and Power Engineering, Nanjing Institute of Technology, No. 1 Hongjing Avenue, Jiangning District, Nanjing 211167, China.
E-mail: xiaoqing_huang@njit.edu.cn

The efficiency of DEC systems is fundamentally tied to the interplay between heat transfer, mass transfer, and airflow dynamics [12]. Early studies focused on porous media as the primary evaporative medium, with materials such as cellulose pads and ceramic foams being widely investigated. For instance, Dai and Sumathy [13] modeled cross-flow DEC systems using honeycomb paper, highlighting the importance of uniform water distribution for thermal homogeneity. Similarly, Ibrahim et al. [14] demonstrated that ceramic-based evaporators exhibit superior wettability but faced challenges in maintaining consistent water flow under variable pressures.

Recent advancements have shifted toward spray-based DEC systems, where nozzle design and operational parameters critically influence performance [15]. Pressure-swirl and impingement atomizing nozzles are commonly employed due to their ability to generate fine droplets, enhancing air-water interfacial contact [16]. However, their study did not address the nonlinear relationship between water supply pressure and cooling efficacy, particularly under fluctuating environmental conditions [17, 18].

Environmental parameters, such as dry-bulb and wet-bulb temperatures, further modulate DEC performance. Chiesa et al. [19] demonstrated that DEC efficiency in Mediterranean climates correlates strongly with wet-bulb depression, achieving peak performance at relative humidity levels below 60%. Saleh and Talib [20] experimentally showed that an indirect evaporative cooling system's performance is influenced by operational parameters such as airflow rate and inlet conditions, achieving effective temperature reduction through optimized design and experimental validation. Yang et al. [21] propose a method for summer design of evaporative cooling systems, considering low-temperature latent heat recovery inefficiencies.

System configuration, including nozzle arrangement and airflow patterns, also plays a pivotal role. Vynnycky and Mitchell [22] modeled the Mpemba effect in evaporative cooling, showing that droplet size and evaporation rate significantly affect thermal equilibration. Zhang et al. [23] conducted an experimental study on a direct evaporative cooler by using the climatic wind tunnel, focusing on its thermal performance. Despite these insights, a comprehensive framework linking nozzle pressure optimization to climatic adaptability remains underdeveloped [24-26].

This study aims to investigate the relationship between water supply pressure and cooling efficiency in DEC spray chambers, with a focus on identifying pressure thresholds that optimize heat and mass transfer dynamics. The work will systematically evaluate how dry-bulb and wet-bulb temperatures, nozzle configurations, and droplet atomization characteristics influence these thresholds.

2. THEORETICAL BASIS FOR THE EXPERIMENT

The spray cooling effect on the air side is calculated using the principles of heat and mass transfer. The reliability and accuracy of the experimental results hinge on the precision of the air side parameters, namely the dry/wet-bulb temperatures. The driving force for heat transfer is the temperature difference, while the driving force for mass transfer is the partial pressure difference of water vapor.

Assuming the air temperature difference dt and the air moisture content difference dm, upon contact between the air and water over an infinitesimal area dA, the sensible heat transfer can be expressed as:

$$dQ_x = Gc_p dt = h(t - t_b)dA \quad (1)$$

where, G represents the air mass flow rate in contact with water [kg/s], c_p is the specific heat capacity of air [J/(kg·°C], h is the surface sensible heat transfer coefficient at the air-water interface [W/(m²·°C)] and t and t_b are the mainstream air temperature and boundary layer air temperature, respectively, [°C].

Moisture transfer can be quantified as follows:

$$dW = Gdm = h_{mp}(P_q - P_{qb})dA \quad (2)$$

where, h_{mp} is the moisture transfer coefficient at the air-water interface and it is determined based on the difference in water vapor partial pressure [kg/(N·s)], P_q and P_{qb} are the water vapor partial pressure in the mainstream air and the boundary layer, respectively [Pa].

The following equation describes the moisture transfer, as the difference in water vapor partial pressure can be approximated by the product of the water content difference and the moisture transfer coefficient over a narrow temperature range:

$$dW = h_{md}(m - m_b)dA \quad (3)$$

Here, h_{md} is the moisture transfer coefficient at the air-water interface is determined by the difference in moisture content [kg/(m²·s], m and m_b are the moisture content in the mainstream air and the boundary layer, respectively [kg/kg].

The latent heat transfer capacity can be determined using the equation below:

$$dQ_q = rdW = rh_{md}(m - m_b)dA \quad (4)$$

where, r is the latent heat of vaporization when the temperature reaches t_b [J/kg].

Eq. (5) is derived based on the total heat transfer capacity $dQ_z = dQ_x + dQ_q$:

$$dQ_z = [h(t - t_b) + rh_{md}(m - m_b)]dA \quad (5)$$

3. Experimental Setup

As shown in Fig. 1, the experimental spray cooling system includes a high-temperature flue system, a ventilation system, and a spray system. The high-temperature flue system comprises a circulating fan, a high-intelligence hot air stove, a wind pipe, and a measuring section. The ventilation system includes an induced draft fan, an exhaust fan, a fan control device, a wind pipe, an air sampler, and a measuring section. The spray system consists of a water tank, a high-pressure water pump, nozzles, a water receiver, and a measuring section.

A rectangular box measuring 2500 mm × 1450 mm × 800 mm was used. Four rows of nozzles were installed on top, with a row spacing of 500 mm and a spacing of 725 mm between nozzles within the same row (see Fig. 1). The water receiver was positioned at the bottom. Pressure-swirl nozzles TF6 and TF8 along with impingement atomizing nozzle AM4 (see Fig. 2) were utilized in the experimentation. The primary parameters and instruments used for measurement are outlined in Table 1. Data was collected every 10 seconds using Fluke equipment.

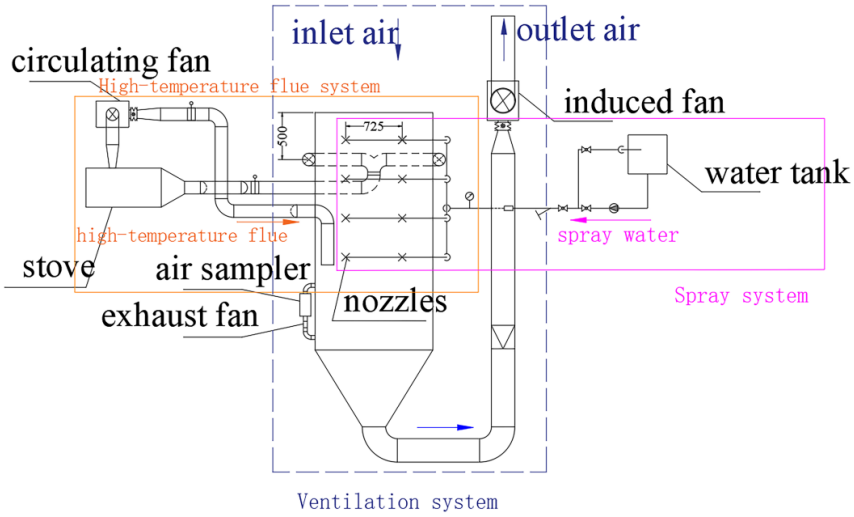

Fig. 1 Schematic diagram of the spray cooling system (Units: mm)

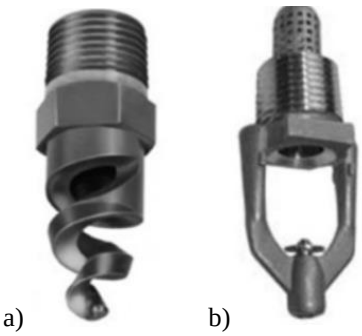

Fig. 2 Schematic diagram of nozzle configurations a) Pressure-swirl nozzles TF6 and TF8 b) Impingement atomizing nozzle AM4

Table 1 Key experimental parameters and instruments

System	Measurement parameters	Instrument	Measuring range
High-temperature flue system	Supply flue temperature	Thermal resistance temperature detector	-70~500 ℃
	Return flue temperature	Thermal resistance temperature detector	-70~500 ℃
	Dynamic pressure of flue pipeline	Pitot tube	2~70 m/s
Ventilation system	Inlet air temperature	Thermograph	-50~70 ℃
	Outlet air temperature	Normal temperature thermocouple×5	-50~70 ℃
	Duct dynamic pressure	Pitot tube	2~70 m/s
	Air sampler dry-bulb temperature	Thermometer×2	0~50 ℃; 50~100 ℃
	Air sampler wet-bulb temperature	Thermometer	0~50 ℃

Spray system	Spray water temperature	Thermometer	0~50 ℃
	Spray water flow	Turbine flow meter LWGY-25 and digit display meter	0~10 m^3/h
	Spray system pressure	Pressure gauge YB150	2.5 MPa, accuracy 0.4
	Droplet diameter	Malvern spraytec particle size analyzer	0.1 μm~2000 μm

4. Heat and Mass Transfer Analysis

The heat and mass transfer processes were analyzed opening TF6 nozzles in row 1 and row 2 (500 mm inter-row spacing, abbreviated as rows 1/2 TF6). Initial chamber inlet conditions showed dry-bulb and wet-bulb temperatures of 80°C and 36.4°C, respectively (Fig. 3).

The dry-bulb temperature decreased substantially with increasing nozzle pressure (0.05-2.00 MPa, 10 increments) and water flow. Thermal equilibrium occurred at 0.70 MPa, where the dry-bulb temperature approached the wet-bulb temperature. Above 0.70 MPa, the cooling rate diminished progressively, exhibiting asymptotic behavior toward the wet-bulb reference state.

This observed equilibrium at 0.70 MPa can be attributed to the competition between enhanced atomization and droplet coalescence. Below this threshold, increased pressure reduces droplet size (Fig. 5), enlarging the air-water interfacial area and improving evaporative cooling efficiency. However, beyond 0.70 MPa, the kinetic energy of droplets surpasses the energy required to overcome surface tension, leading to frequent droplet collisions and coalescence (Fig. 6). Larger droplets reduce the effective contact area, thereby diminishing both latent heat transfer and cooling performance. This phenomenon aligns with the findings of Zhao et al. [16], who noted similar saturation effects in spray cooling systems under high-pressure conditions.

Fig. 4 illustrates the heat and mass transfer processes in rows 1/2 TF6. Initially, the sensible heat transfer (Q_x) decreased with increasing water pressure, reaching equilibrium at a nozzle pressure of 0.70 MPa, exhibiting a trend similar to the dry-bulb temperature. The latent heat transfer (Q_q) increased with rising water content and nozzle pressure but decreased at a water supply pressure of 0.70 MPa due to air dehumidification. And the total heat transfer (Q_z) was in balance, but it subsequently decreased. Before air saturation, evaporative cooling is the dominant driving force of spray cooling. However, after the water supply pressure reaches 0.70 MPa, heat convection between air and water becomes the dominant force. In terms of water conservation, evaporative cooling should be prioritized. Furthermore, the reduction in dry-bulb temperature is not significant when the water supply pressure reaches 0.70 MPa. Therefore, the optimal spray cooling pressure for TF6 is determined to be 0.7 MPa. Beyond this pressure, increasing the spray quantity in the humidification chamber does not significantly reduce the dry-bulb temperature.

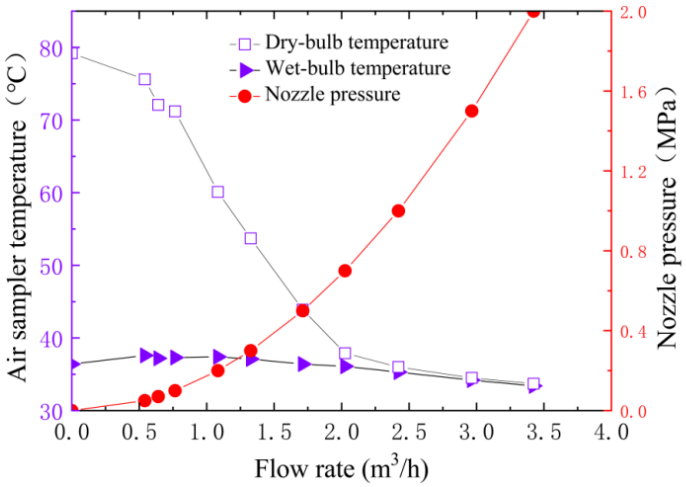

Fig. 3 Variation in air sampler temperature in rows 1/2 TF6

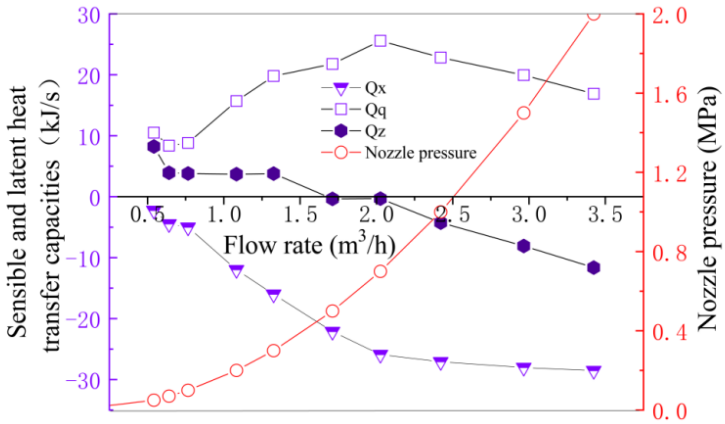

Fig. 4 Heat and mass transfer processes in rows 1/2 TF6

The transition from evaporative cooling to convective dominance highlights a critical trade-off in DEC system design. While higher pressures initially enhance moisture transfer, excessive humidity saturation (approaching 100% relative humidity) limits further evaporation, as shown by the decline in Q_q beyond 0.70 MPa (Fig. 4). This behavior corroborates the theoretical model in Eq. (4), where latent heat transfer depends on the vapor pressure gradient. Once the air nears saturation, the gradient diminishes, reducing Q_q. Practical implications suggest that maintaining pressure near 0.70 MPa optimizes both energy efficiency and water conservation, particularly in high-temperature applications.

A curve depicting the variation in atomized droplet diameters (explained in Table 2) of the TF6 nozzle, measured 7 cm below the nozzle, with spray pressure was plotted based on the results obtained using the Malvern method, as shown in Fig. 5.

Table 2 Definitions of atomized droplet diameters

Symbol	Name	Meaning
$D_{[3][2]}$	Sauter mean diameter (SMD)	The ratio of the total volume of droplets to their total surface area.
$D_{[4][3]}$	Mass mean diameter (MMD)	The ratio of the total mass of droplets to their total volume.
$D_{v(10)}$		The volume of droplets with diameters smaller than $D_{v(10)}$ accounts for 10% of the total droplet volume.
$D_{v(50)}$	Mass median diameter	The volume of droplets with diameters smaller than $D_{v(50)}$ accounts for 50% of the total droplet volume. This corresponds to the point where the areas under the volume distribution curve on both sides of $D_{v(50)}$ are equal.
$D_{v(90)}$		The volume of droplets with diameters smaller than $D_{v(90)}$ accounts for 90% of the total droplet volume.

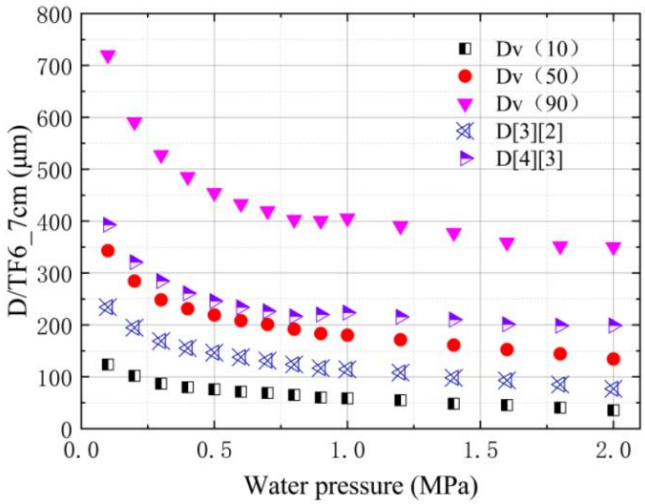

Fig. 5 Variation in atomized droplet diameters of the TF6 nozzle with increased water pressure

The distribution of atomized droplet diameters, as depicted in Fig. 5, shows that $D_{V[9][0]}$ is the maximum value, followed by $D_{[4][3]}$, $D_{V[5][0]}$ and $D_{[3][2]}$ in descending order, with $D_{V[1][0]}$ being the minimum.

The minimal reduction in droplet diameter beyond 0.70 MPa (Fig. 5) further supports the hypothesis of energy redistribution. As pressure increases, excess kinetic energy no longer contributes to atomization but instead accelerates droplet motion, promoting collisions. This aligns with the observations of Zhang et al. [23], who emphasized the role of nozzle-generated turbulence in droplet dynamics. Notably, the Sauter mean diameter ($D_{[3][2]}$) – a critical parameter for interfacial area – plateaus beyond 0.70 MPa, indicating diminishing returns in heat transfer enhancement.

5. OPTIMAL WATER SUPPLY PRESSURE

During the experimental process, a specific water supply pressure was identified for each type of TF6, TF8, and AM4 nozzles. For each type of nozzle, if the dry-bulb temperature of the air did not significantly decrease as the water pressure exceeded this specific level, it indicated the existence of an optimal water supply pressure for the spray cooling process. The optimal water supply pressure for a humid chamber is defined as the pressure at which the dry-bulb temperature of the air no longer decreases significantly and approaches the wet-bulb temperature after the nozzles' back-pressure reaches a certain value. Table 3 presents the optimal water supply pressures for various types of nozzles and different nozzle arrangements.

Table 3 Optimal water supply pressures

Nozzle types	Arrangements	Dry-bulb temperatures at the air inlet	Optimal water supply pressures
TF6	725 mm×725 mm 500 mm×500 mm 500 mm×725 mm	38˚C	0.55 MPa
TF6	725 mm×725 mm 500 mm×500 mm 500 mm×725 mm	80˚C	0.70 MPa
TF8	725 mm×725 mm 500 mm×500 mm 500 mm×725 mm	38˚C	0.35 MPa
TF8	725 mm×725 mm 500 mm×500 mm 500 mm×725 mm	80˚C	0.50 MPa
AM4	725 mm×725 mm 500 mm×500 mm 500 mm×725 mm	38˚C	0.25 MPa
AM4	725 mm×725 mm 500 mm×500 mm 500 mm×725 mm	80˚C	0.35 MPa

5.1 Optimal Water Supply Pressure Variation with Dry-Bulb Temperature at Air

Table 3 indicates an increase in optimal water supply pressure with rising dry-bulb temperature at the air inlet. Nonetheless, the increase was limited for each nozzle type. Fig. 6 depicts droplet size distribution 7 cm below a TF6 nozzle across various water supply pressures.

When the water supply pressure exceeded 0.8 MPa, the Spraytec analyzer detected droplets larger than 1,000 μm. Both the number and diameter of these droplets increased with further pressure increases. Analyzing from the perspective of droplet atomization energy conservation, the change in droplet diameter was insignificant once the nozzle back-pressure reached 0.7-0.8 MPa. Hence, it is inferred that the work to overcome surface tension and viscous forces remained constant, with excess energy converting to droplet kinetic energy. The increased kinetic energy led to more droplet collisions, forming larger droplets detrimental to heat and mass transfer.

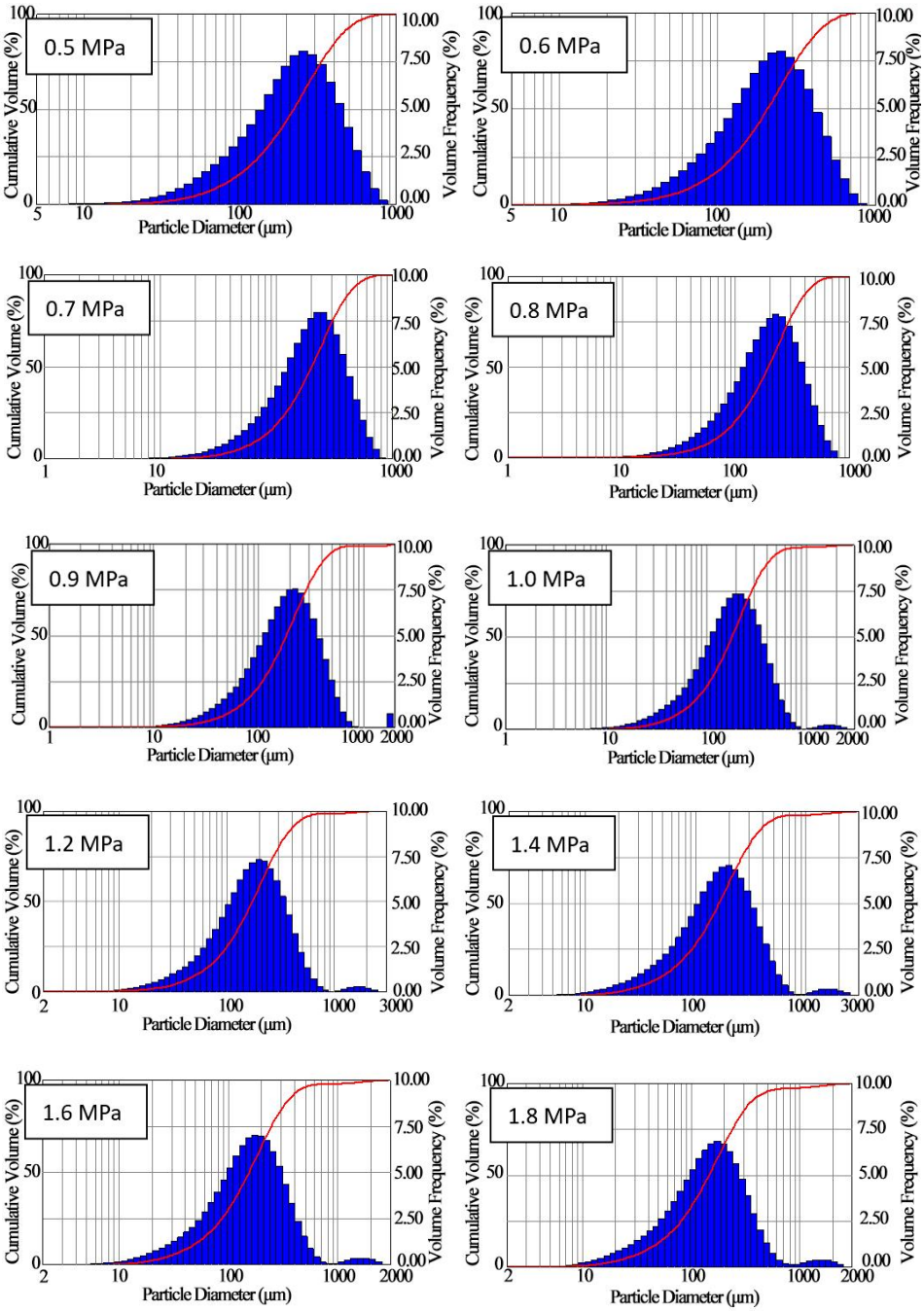

Fig. 6 Droplet size distribution 7 cm below a TF6 Nozzle at various water supply pressures

5.2 Impact of Wet-Bulb Temperature on Optimal Water Supply Pressure

Fig. 7 displays the variation in the air cooling effect of TF6 nozzles arranged in a 500 mm×725 mm layout, with an air inlet dry-bulb temperature of 80°C, considering the product of the difference between dry/wet-bulb temperatures and the evaporation rate. The analysis indicates that the optimal water supply pressure remained stable at approximately 0.7 MPa within the high-temperature range. Consequently, the wet-bulb temperature had an insignificant impact on the optimal water supply pressure.

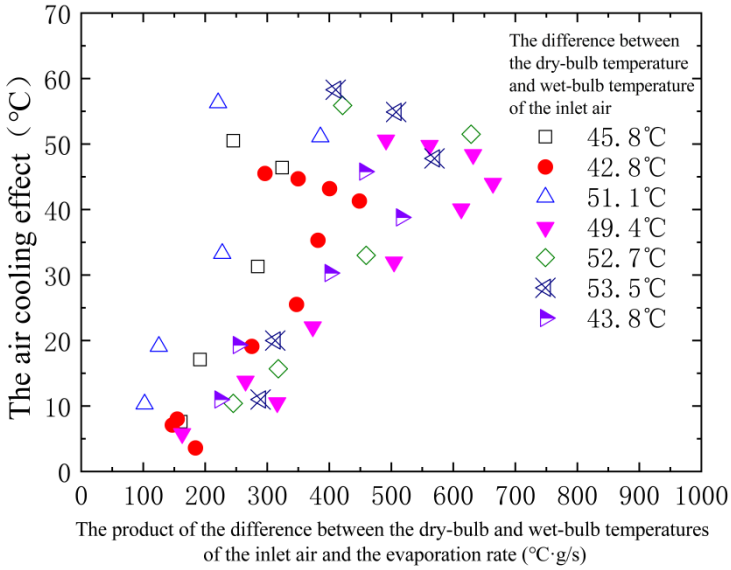

Fig. 7 The air cooling effect in relation to the product of the difference between the dry-bulb and wet-bulb temperatures of the inlet air and the evaporation rate

Table 3 demonstrates that when using the same type of nozzle to cool air with identical parameters, variations in the TF6 nozzle arrangement had no impact on the optimal water supply pressure.

6. CONCLUSION

This study experimentally investigated the heat and mass transfer dynamics in direct evaporative cooling (DEC) spray chambers, focusing on the identification of optimal water supply pressures for three nozzle types (TF6, TF8, AM4). Through systematic analysis of spray cooling efficacy under varying operational and environmental conditions, the work establishes critical relationships between pressure thresholds, nozzle characteristics, and cooling performance.

Key findings are summarized as follows:

- Existence of optimal water supply pressure: Increasing water supply pressure beyond a critical threshold (e.g., 0.70 MPa for TF6) reduced cooling efficiency due to excessive droplet coalescence and humidity saturation (Fig. 4).
- Nozzle Specific Pressure Thresholds: Experimental data analysis identified distinct optimal pressures for TF6, TF8, and AM4 nozzles under various conditions.

Future research should prioritize the development of real-time control algorithms that dynamically adjust water supply pressure based on meteorological forecasts, thereby enhancing climatic adaptability.

Additionally, integrating experimental findings with computational fluid dynamics (CFD) simulations could advance predictive models for multiphase flow behavior under transient airflow conditions, enabling more robust optimization of DEC systems.

REFERENCES

1. Guan, L., Bennett, M., Bell, J., 2015, *Evaluating the potential use of direct evaporative cooling in Australia*, Energy and Buildings, 108, pp. 185-194.
2. Heidarinejad, G., Farahani, M. F., Delfani, S., 2010, *Investigation of a hybrid system of nocturnal radiative cooling and direct evaporative cooling*, Building and Environment, 45(6), pp. 1521-1528.
3. Saleem, J., Chahrour, K. M. N., 2024, *Enhancing the Efficiency of Air Conditioning Systems in High-Temperature Climates Through Direct Evaporative Cooling*, Journal of Sustainability for Energy, 3(2), pp. 119-138.
4. Farmahini-Farahani, M., Delfani, S., Esmaeelian, J., 2012, *Exergy analysis of evaporative cooling to select the optimum system in diverse climates*, Energy, 40(1), pp. 250-257.
5. Tayawade, A. N., Gayakwad, H. R., Kale, P. B., 2010, *Study on roof ventilation and misting system in semicontrolled polyhouse*, New Agriculturist, 21(1,2), pp. 65-68.
6. Gürdil, G. A. K., Demirel, B., Kic, P., Yaylagül, E. D., 2020, *Design and construction of a farm scale evaporative cooling system*, Agricultural Mechanization in Asia, Africa and Latin America: AMA, 51(2), pp. 67-71.
7. Hamlin, S., Hunt, R., Tassou, S. A., 1998, *Enhancing the performance of evaporative spray cooling in air cycle refrigeration and air conditioning technology*, Applied Thermal Engineering, 18(11), pp. 1139-1148.
8. Lekwuwa, C. J., Ogbu, A. C., Hubert, A. C., Chukwulozie, O. P., 2012, *A mathematical model of an evaporative cooling pad using sintered Nigerian clay*, Journal of Minerals and Materials Characterization and Engineering, 11(11), pp. 1113-1120.
9. Halasz, B., 1998, *A general mathematical model of evaporative cooling devices*, Revue Générale de Thermique, 37(4), pp. 245-255.
10. Beshkani, A., Hosseini, R., 2006, *Numerical modeling of rigid media evaporative cooler*, Applied Thermal Engineering, 26(5-6), pp. 636-643.
11. Liu, T., Pang, H., He, S., Zhao, B., Zhang, Z., Wang, J., Liu, Z., Huang, X., Shi, T., Gao, M., 2023, *Evaporative cooling applied in thermal power plants: a review of the state-of-the-art and typical case studies*, Fluid Dynamics & Materials Processing, 19(9), pp. 2229-2265.
12. Fouda, A., Melikyan, Z., 2011, *A simplified model for analysis of heat and mass transfer in a direct evaporative cooler*, Applied Thermal Engineering, 31(5), pp. 932-936.
13. Dai, Y. J., Sumathy, K., 2002, *Theoretical study on a cross-flow direct evaporative cooler using honeycomb paper as packing material*, Applied Thermal Engineering, 22(13), pp. 1417-1430.
14. Ibrahim, E., Shao, L., Riffat, S.B., 2003, *Performance of porous ceramic evaporators for building cooling application*, Energy and Buildings, 35(9), pp. 941-949.
15. Zhang, K., Zhu, X., Ren, X., Qiu, Q., Shen, S., 2017, *Numerical investigation on the effect of nozzle position for design of high performance ejector*, Applied Thermal Engineering, 126, pp. 594-601.
16. Zhao, R., Cheng, W. L., Liu, Q. N., Fan, H. L., 2010, *Study on heat transfer performance of spray cooling: model and analysis*, Heat and Mass Transfer, 46, pp. 821-829.
17. Liu, Q., Guo, C., Wu, Z., You, Y., Li, Y., 2022, *Heat and mass transfer model optimization and annual energy efficiency analysis for energy recovery indirect evaporative cooling*, Building Simulation, 15(7), pp. 1353-1365.

18. Kavaklioglu, K., Koseoglu, M.F., Caliskan, O., 2018, *Experimental investigation and radial basis function network modeling of direct evaporative cooling systems*, International Journal of Heat and Mass Transfer, 126, pp. 139-150.
19. Chiesa, G., Huberman, N., Pearlmutter, D., 2019, *Geo-climatic potential of direct evaporative cooling in the Mediterranean Region: A comparison of key performance indicators*, Building and Environment, 151, pp. 318-337.
20. Saleh, A.A.M., Talib, S.S.A., 2018, *Experimental investigation of an indirect evaporative cooling system*, Journal of Engineering & Applied Sciences, 13(20), pp. 381-392.
21. Yang, Y., Huang, X., Chu, J., Li, H., Yang, L., 2024, *Generating method of outdoor design parameter for evaporative cooling air conditioning*, Journal of Refrigeration, 45(3), pp. 104-111.
22. Vynnycky, M., Mitchell, S.L., 2010, *Evaporative cooling and the Mpemba effect*. Heat and Mass Transfer, 46, pp. 881-890.
23. Zhang, L., Feng, Y., Meng, Q., Zhang, Y., 2015, *Experimental study on the building evaporative cooling by using the Climatic Wind Tunnel*, Energy and Buildings, 104, pp. 360-368.
24. Smith, S.T., Hanby, V.I., Harpham, C., 2011, *A probabilistic analysis of the future potential of evaporative cooling systems in a temperate climate*, Energy and Buildings, 43(2-3), pp. 507-516.
25. Shteling, V.S., Dedov, A.V., Zakharenkov, A.V., Komov, A T., Shcherbakov, P.P., 2022, *An experimental study of wall thermal stabilization efficiency by spray cooling*, Thermal Engineering, 69(12), pp. 954-962.
26. Jain, J.K., Hindoliya, D.A., 2011, *Experimental performance of new evaporative cooling pad materials*, Sustainable Cities and Society, 1(4), pp. 252-256.